Adaptive extended kalman filter for PEMFC membrane water content estimation

Gontran Lance, Thomas Leroy, Jules Sery

International Journal of Hydrogen Energy 71 (2024) 1164–1173

Contents lists available at ScienceDirect

International Journal of Hydrogen Energy

journal homepage: www.elsevier.com/locate/he

Adaptive extended kalman filter for PEMFC membrane water content estimation

Gontran Lance *, Thomas Leroy, Jules Sery

IFP Energies nouvelles, Institut Carnot IFPEN Transports Energie, 1 et 4 avenue de Bois-Préau, 92852 Rueil-Malmaison, France

ARTICLE INFO

Handling Editor: Suleyman I. Allakhverdiev

Keywords:
PEMFC
Membrane water content
Software sensor
Extended kalman filter
Real-time capable

ABSTRACT

Proton Exchange Membrane Fuel Cells are a favorite technology for decarbonizing the transportation sector. However, their large-scale democratization is hampered by their high cost compounded by their unsatisfactory lifespan. To anticipate potential degradation while keeping improving performance, it is essential to maintain an acceptable humidity range inside the cells, especially at the membrane level. However, membrane humidity level is not directly measurable, alternative techniques must be considered to recover this key variable. Here, we develop a real-time software sensor of the membrane water content at the fuel cell's heart. We build a model describing the membrane water balance, electrochemical behavior, and species mass balance. We then reduce the model and perform an Adaptive Extended Kalman Filter. We perform sensitivity analyses in both steady-state and transient conditions. We validate the filter on a "Worldwide Harmonized Light Vehicles Test Cycles" test procedure. Finally, we obtain a fast and accurate model-based software sensor.

1. Introduction

Addressing the challenge of finding new energy sources and carriers is crucial for reducing global greenhouse gas emissions. Hydrogen is a promising alternative for certain uses, such as freight, rail, or maritime transport, provided that its production results in sufficiently low carbon emissions [1]. In this context, the Polymer Electrolyte Membrane Fuel Cell (PEMFC) is currently the subject of intensive and extensive research. It is one of the preferred technologies for decarbonizing the transport sector, especially for heavy transport vehicles, due to its autonomy and ease of recharging. The main limitations to the dissemination of this technology are its lifetime and cost. Although technological improvements span across many domains, this paper specifically focuses on advanced system control strategies. The aim is to enhance the use and lifetime of a fuel cell while preventing further damages.

Controlling a Proton-Exchange Membrane Fuel Cell (PEMFC) involves managing the supply of reactants (oxygen and hydrogen) to the membrane while controlling their thermodynamic states (pressure, temperature, and humidity). Sensors are available in the air and hydrogen systems to enable proper management of the fuel cell. However, certain inner states of the fuel cell that could be advantageous for control strategies are not always accessible due to technical complexity or the cost of measurement devices. One important example of a valuable inner state is the water content of the membrane.

Understanding the behavior of the water content of the membrane is crucial for monitoring proton conductivity and fuel cell performance during a mission profile. Additionally, the membrane water content is important for degradation assessment. A dry membrane can lead to increased electrical resistance and a higher likelihood of pinhole degradation, as explained in Ref. [2]. On the contrary, if the membrane is too wet, it can flood the cathode diffusive layer, leading to a decrease in performance and accelerated degradation [3]. Monitoring the water content of a PEMFC is a necessary and challenging objective. There are several methods for estimating the water content of the membrane.

Ohmic resistance measurement. Knowledge of ohmic losses in voltage can provide relevant information on the water content of the membrane. Recent research papers have focused on reconstructing the membrane water content using the ohmic resistance of the fuel cell. In Ref. [4], the authors develop an estimator for the membrane water content of a fuel cell. This is achieved by using a water transport model and measuring fuel cell impedance through EIS (Electrochemical Impedance Spectroscopy), as well as inlet and exhaust gas concentrations on the anode and cathode sides. A recent overview of EIS sensors for fuel cell applications can be found in Ref. [5]. However, prior planning is necessary to integrate the sensor into the system and estimate additional costs.

Ohmic resistance estimation. Designing a state observer of the ohmic

* Corresponding author.
E-mail addresses: gontran.lance@ifpen.fr (G. Lance), thomas.leroy@ifpen.fr (T. Leroy), jules.sery@gmail.com (J. Sery).

https://doi.org/10.1016/j.ijhydene.2024.05.199
Received 16 February 2024; Received in revised form 26 April 2024; Accepted 13 May 2024
Available online 25 May 2024

resistance can eliminate the need for a sensor to calculate the membrane water content. In Ref. [6], instead of measuring the fuel cell impedance, the authors design an Extended Kalman Filter for its real time reconstruction. In Ref. [7], the authors present a 2D model of a PEMFC and construct an Extended Kalman Filter as a state observer to estimate the evolution of the concentrations of the various species in the cathode-side stack, as well as the ohmic resistance. In Ref. [8], a double Kalman filter can be used to estimate the ohmic resistance of the fuel cell based on measurements of the cell's output voltage and current. The equation that relates the water content of the membrane to the ohmic resistance can be inverted to determine the water content. However, reducing the estimate of water inside the fuel cell to its link with ohmic resistance is an incomplete approximation. It is more informative to strengthen this connection by incorporating a physical model of water transport phenomena.

Abbreviations and nomenclature

α	Cathode transfer coefficient
ΔH	Reaction LHV at STP $\left(-241.83\,kJ.mol^{-1}\right)$
ΔS	Entropy of reaction at STP $\left(-163.34JK^{-1}mol^{-1}\right)$
γ	Kinetic reaction order
σ_p	Ionomer protonic conductivity $\left(Scm^{-1}\right)$
a_a	Membrane absorption coefficient $\left(cms^{-1}\right)$
a_d	Membrane desorption coefficient $\left(cms^{-1}\right)$
c_f	Concentration of fixed charge sites $\left(molm^{-3}\right)$
E_{act}	Catalytic activation energy $\left(J.mol^{-1}\right)$
E_{rev}	Theoretical reversible voltage (V)
F	Faraday constant $\left(Asmol^{-1}\right)$
j	Cell current density $\left(Acm^{-2}\right)$
j_L	Limiting current density $\left(Acm^{-2}\right)$
$j0_{ref}$	Exchange current density at reference conditions P_{ref} and T_{ref} $\left(Acm^{-2}\right)$
N_{cell}	Cell's number
P_X	Partial pressure of species X in gas channel (Pa)
R	Universal gas constant $\left(8.314JK^{-1}mol^{-1}\right)$
S_{cell}	Active surface area $\left(cm^2\right)$
x_m	Membrane thickness (m)
x_{CL}	Catalyst Layer thickness (m)
x_{GDL}	Gas Diffusion Layer thickness (m)
CL	Catalyst Layer
GDL	Gas Diffusion Layer

Direct humidity estimation. The objective of this task is to design a state observer that can estimate fuel cell humidity using a representative physical model of the water dynamics with well-chosen and easily measurable outputs. In the context of PEMFC simulation, it is essential to consider the nonlinear modeling, which includes the electrochemical, liquid, and gas transport phenomena inside the multiple constitutive layers of a PEMFC. In Ref. [9], the authors employ a Luenberger observer to estimate the various species present in the cathode and anode gas channels. They then use this information to deduce the membrane water content. A similar methodology is found in Ref. [10]. On the other hand, if we can compute first-order derivatives, the Extended Kalman Filter is well-suited for nonlinear systems. In Ref. [11], the authors develop a constrained Extended Kalman Filter that incorporates species dynamics in multiple layers and water activity in the membrane. This model has the advantage of working in challenging operating conditions, such as start-up and shutdown. Water modeling is straightforward, as it only calculates the average water activity between the anode and cathode. In Ref. [12], the authors address the issue of determining cathode flooding in PEMFCs using a model-based approach combined with an Unscented Kalman Filter. This filter is derived from the usual Kalman observer, but has the advantage of not requiring a Jacobian, which would slow down computation time. The method is typically more robust but does not converge exponentially. In Ref. [13], the authors build a high-order model-based sliding mode observer with chattering capabilities to recover the temperature of the fuel cell and the liquid saturation. The chosen model requires many parameters to be tuned for real operations. Besides, in Ref. [14], the authors introduce an observer to estimate liquid water in the catalyst layer. In Ref. [15], the authors design a novel observer based on an extended Kalman filter and a specific differential detectability property to estimate both the temperature and the liquid saturation at the cathode catalyst layer. The previous observers do not account for water membrane dynamics. In Ref. [16], the authors aim to reconstruct both gas species and membrane water content using a sliding mode observer based on anode pressure and membrane resistance measurements. Several articles have highlighted the effectiveness of sliding-mode observers (SMOs) in estimating various inner states of PEMFC. For example, in Ref. [17], the authors construct a state observer for estimating membrane water content. This observer is based on an empirical dynamic voltage model. They then use a sliding-horizon observer and close the loop with voltage measurements. Then, they recover the membrane content by inverting the relationship between ohmic losses and membrane water content. In Ref. [18], the authors construct an adaptive sliding-horizon observer, based on an empirical electrochemical model. They then recover the relative humidity by inverting an equation that links it to the fuel cell voltage. From data-based side, we can find in Ref. [19] a dynamic partial least squares regression method to predict the moisture content of the fuel cell membrane. The algorithm is trained using measurements of voltage, current, and relative humidity at both the anode and cathode. In Ref. [20], the authors suggest an adaptive sliding mode estimation algorithm with operational conditions to recover the humidity conditions of the cathode and anode. In Ref. [21], the authors present an update with an adaptive sliding mode observer thanks to a third-order PEMFC humidity model that considers membrane water dynamics. The humidity observer focuses on water pressures in the anode and cathode volumes, as well as membrane water content. However, the current literature still presents simple models where the membrane's water management process is not accurately modeled. Additionally, most literature on fuel cell humidity uses 1D modeling, but more precise information would be beneficial.

To address the underlined issues, this paper specifically focuses on determining the water content in the membrane using easily obtainable measurements. One possible relevant contribution that has not yet been explored for estimating water content is the use of a state observer based on a model that considers the main water transport effects that occur in the membrane, such as diffusion, electroosmotic effect, and sorption phenomena, using a three-point discretization in the through-the-membrane direction to accurately capture the water content at the core of the membrane. We utilize an implicit nonlinear observer model as our observation strategy. This model is based on an adaptive Extended Kalman Filter, which was inspired by Ref. [22]. This paper presents a non-binding estimate of water content within the membrane, based solely on reachable measurements such as PEMFC voltage and current.

The paper is structured as follows: Section 2 introduces the PEMFC plant model, which consists of three parts: electrochemical modeling, membrane water content system, and mass balance equations. Section 3 presents the reduced model, and Section 4 describes the resulting adaptive Extended Kalman Filter. The article concludes in Section 5 with numerical examples that demonstrate the effectiveness of the designed observer.

2. PEMFC model

The following assumptions are made for the PEMFC model considered in this work.

- The cell is isothermal, and the temperature is a given parameter.

- No liquid water transport in Gas Diffusion Layers (GDL) is considered in this work.
- A hydrogen recirculation loop is modeled with either an active (pump) or passive (ejector) system.
- Gas diffusion transport in all cell layers is considered in steady state at each time step.
- Proton conductivity and oxygen diffusion in the Catalyst Layers (CL) are assumed being infinitely fast.
- The activation overpotential is negligible at the anode considering an infinitely fast hydrogen oxidation reaction.
- The ohmic losses are located only in the membrane and the electrical conductivity of the other layers are assumed to be infinitely high.
- We model the cathode and anode gas channels as lumped control volumes and the evolution of reactants concentration in the along-the-channel direction is neglected.
- Water produced by the oxygen reduction reaction ends up directly into the cathode GDL.
- The gases in all cell layers are considered as perfect gases.

Throughout Section 2, space variable x denotes the through-the-membrane direction.

2.1. Electrochemical model

The average cell voltage within the stack can be written as

$$E_{cell} = E_{rev} - \eta_{act} - \eta_{conc} - \eta_{\Omega}, \tag{1}$$

with E_{rev} the reversible voltage, η_{act} the activation losses, η_{conc} the concentration losses and η_{Ω} the ohmic losses. From Ref. [23], the theoretical reversible voltage (or open-circuit voltage) is a function of the temperature, pressure and concentration

$$E_{rev} = -\left(\frac{\Delta H}{2F} - \frac{T\Delta S}{2F}\right) + \frac{RT}{2F}\ln\left[\frac{\frac{P^a_{H_2}}{P_{ref}}\left(\frac{P^c_{O_2}}{P_{ref}}\right)^{\frac{1}{2}}}{\frac{P^c_{H_2O}}{P_{sat}(T)}}\right], \tag{2}$$

with ΔH and ΔS the reaction lower heating value and entropy of reaction at standard temperature and pressure. T indicates the stack temperature. $P^a_{H_2}$ and $P^a_{H_2O}$ denote the hydrogen and water partial pressures in the anode volume. $P^c_{O_2}$ and $P^c_{H_2O}$ refer to the oxygen and water partial pressures in the cathode volume. P_{ref} is the reference pressure and $P_{sat}(T)$ is the saturation pressure as a function of the temperature. Finally, F and R are the Faraday and universal gas constants.

2.1.1. Activation losses

The activation overvoltage accounts for the energy required to drive the oxygen reduction reaction because its chemical kinetics are very slow as compared to the hydrogen oxidation reaction. Therefore, the activation overpotential at the anode is neglected in this model. The Butler-Volmer kinetics are reduced to the Tafel equation (see Ref. [23])

$$\eta_{act} = \frac{RT}{\alpha F}\ln\left[\frac{j}{j_0}\right], \tag{3}$$

with α the cathode transfer coefficient and j the cell current density. We denote by j_0 the exchange current density being a function of oxygen partial pressure and temperature within the cathode catalyst layer, which we express as

$$j_0 = j_{0_{ref}}\left(\frac{P^c_{O_2}}{P_{O_2,ref}}\right)^{\gamma}\exp\left[\frac{E_{act}}{R}\left(\frac{1}{T_{ref}} - \frac{1}{T}\right)\right], \tag{4}$$

with $j_{0_{ref}}$ and $P_{O_2,ref}$ the exchange current density and the O_2 reference pressure respectively at reference conditions P_{ref} and T_{ref}. $P^c_{O_2}$ denotes the O_2 partial pressure at the cathode side. E_{act} and γ respectively refer to the catalytic activation energy and the kinetic reaction order.

2.1.2. Concentration losses

The concentration losses account for the transport of O_2 from the bipolar plate to the CL. We follow [23] and write the concentration losses as

$$\eta_{conc} = -\frac{RT}{\alpha F}\ln\left(1 - \frac{j}{j_L}\right). \tag{5}$$

The diffusion is assumed to be very fast, and the steady-state assumption is made so that the oxygen consumption in the CL is equal to the diffusion flux through the cathode

$$\frac{j}{4F} = -\frac{D_{O_{2_{eff}}}}{RT}\frac{\partial P_{O_2}}{\partial x}, \tag{6}$$

with $D_{O_{2_{eff}}}$ the effective diffusion coefficient. To make appear the limiting current density, we then compute the oxygen partial pressure at the CL with (6) as a function of the oxygen partial pressure in the cathode gas channel $P^c_{O_2}$.

$$P^{CL}_{O_2} = P^c_{O_2} - \frac{jRTx_{GDL}}{4FD_{O_{2_{eff}}}} = P^c_{O_2}\left(1 - \frac{j}{j_L}\right). \tag{7}$$

with x_{GDL} the gas diffusion layer thickness. The limiting current density consequently writes $j_L = 4FD_{O_{2_{eff}}}P^c_{O_2}/RTx_{GDL}$. The effective diffusion coefficient reads

$$D_{O_{2_{eff}}} = \frac{\epsilon}{\tau^2}D_{O_2}, \tag{8}$$

where ϵ and τ are the GDL porosity and tortuosity respectively. In Section 5, we specify the bulk oxygen diffusion coefficient in the cathode gas channel D_{O_2}.

2.1.3. Ohmic losses

The ohmic voltage losses involved in (1) write

$$\eta_{\Omega} = j\int_0^{x_m}\frac{dx}{\sigma_p(\lambda_m)}, \tag{9}$$

where σ_p denotes the protonic conductivity of the membrane as a function of the membrane water content λ_m defined below and x_m referring to the membrane thickness.

2.2. Membrane model

To find the water content profile inside the membrane, a water transport model is used. We define λ as the dimensionless variable standing for the water concentration in the membrane c_w over the concentration of fixed charge sites c_f such that

This model includes the water diffusion inside the membrane, the electroosmotic drag of water molecules due to proton transport and the absorption and desorption of water at both membrane/CL interfaces.

The water content profile inside the membrane is discretized according to a three-point spatial approximation as shown in Fig. 1. The water content is assumed to be uniform inside the cathode and anode CLs and GDLs. Based on the various transport phenomena described in Ref. [24] and the steady-state equation described in Ref. [25], the water balance inside the membrane is given by the following partial differential equation defined in both the membrane and the catalyst layers

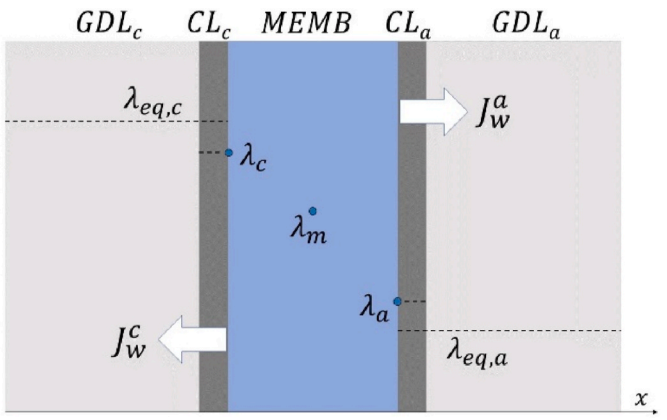

Fig. 1. *Space discretization of membrane water content. Indexes c, m, a respectively stand for cathode, membrane, and anode.*

$$\lambda = \frac{c_w}{c_f}. \tag{10}$$

$$\frac{\partial \lambda}{\partial t} = \frac{\partial}{\partial x}\left(D(\lambda)\frac{\partial \lambda}{\partial x} + \frac{n_d(\lambda)}{c_f F} j\right) + J_w(\lambda), \tag{11}$$

with c_f as the concentration of fixed charge sites which depends on the type of membrane chosen (e.g., SO_3^- ions). J_w denotes the water fluxes at both electrode membrane interfaces such that

$$J_w(\lambda) = \begin{cases} k_{ad}(\lambda) c_f \left(\lambda_{eq}(P_{H_2O}, T) - \lambda\right) \text{ in CLs}, \\ 0 \text{ in the membrane}. \end{cases} \tag{12}$$

A constant water content is considered inside the catalyst layers of both anode and cathode, characterized by the equilibrium water content λ_{eq}, which defines an equivalent water content in both CLs depending on the water vapor activity $a_{H_2O} = P_{H_2O}/P_{sat}(T)$. The water system (11) is a nonlinear partial differential equation, which we spatially discretize according to a second order scheme for a sake of real-time capable computing, first using a centered finite difference scheme for the first partial derivative and a three-point approximation for the spatial derivative of the diffusive terms. This leads to a rewrite of (11) with the three-dimensional vector $\lambda = (\lambda_a \quad \lambda_m \quad \lambda_c)^T$ through the ordinary differential equations:

$$\frac{d\lambda}{dt} = \frac{D(\lambda)}{x_m} A_\lambda \lambda + \frac{1}{c_f x_{CL}} \begin{pmatrix} -\frac{n_d(\lambda)}{F} j + J_w^a(\lambda) \\ 0 \\ \frac{n_d(\lambda)}{F} j + J_w^c(\lambda) \end{pmatrix}, \tag{13}$$

where $A_\lambda = \begin{pmatrix} -\frac{3}{x_{CL}} & \frac{4}{x_{CL}} & -\frac{1}{x_{CL}} \\ \frac{4}{x_m} & -\frac{8}{x_m} & \frac{4}{x_m} \\ -\frac{1}{x_{CL}} & \frac{4}{x_{CL}} & -\frac{3}{x_{CL}} \end{pmatrix}$ denotes the resulting spatial discretization matrix of transport terms, x_{CL} and x_m the thicknesses of both the membrane and catalyst layers. The resulting water fluxes at the membrane/CL interfaces read

$$\begin{cases} J_w^a(\lambda) = k_{ad}(\lambda_a) c_f \left(\lambda_{eq}^a\left(P_{H_2O}^a, T\right) - \lambda_a\right), \\ J_w^c(\lambda) = k_{ad}(\lambda_c) c_f \left(\lambda_{eq}^c\left(P_{H_2O}^c, T\right) - \lambda_c\right), \end{cases} \tag{14}$$

with both λ_{eq}^c and λ_{eq}^a that depend on the fuel cell type and are defined for numerical applications in Section 5. Unlike the membrane modeling defined in Ref. [21], we obtain a three-point discretization of the membrane water content, which can be more representative of the sorption phenomenon.

2.3. Molar balance model

In addition to the electrochemical and membrane modeling, we also account for the molar balance of the various key species involved in the fuel cell.

2.3.1. Cathode gas channel model

In the cathode gas channel, oxygen is consumed and the membrane exchanges water with the gas channel. The species molar balance modifies the oxygen and water partial pressures $P_{O_2}^c$ and $P_{H_2O}^c$ in the cathode volume through the equations

$$\begin{cases} \frac{dP_{O_2}^c}{dt} = \frac{RT}{V_c}\left(W_c^{in} X_{O_2}^{in} - \frac{S_{cell} N_{cell}}{4F} j - W_c^{out} \frac{P_{O_2}^c}{P_c}\right), \\ \frac{dP_{H_2O}^c}{dt} = \frac{RT}{V_c}\left(W_c^{in} X_{H_2O}^{in} - W_c^{out} \frac{P_{H_2O}^c}{P_c} + \frac{S_{cell} N_{cell}}{2F} j \right. \\ \qquad \left. - J_w^c S_{cell} N_{cell}\right). \end{cases} \tag{15}$$

T stands for the temperature in the cathode volume and V_c refers to the volume considered for the cathode side. S_{cell} is the area of the cell and N_{cell} is the number of cells in the stack. W_c^{in} and W_c^{out} refer to the cathode inlet and outlet molar flows. $X_{H_2O}^{in}$ and $X_{O_2}^{in}$ are the cathode inlet molar fractions defined by

$$\begin{cases} X_{H_2O}^{in} = HR_c \frac{P_{sat}(T)}{P_c}, \\ X_{O_2}^{in} = X_{O_2}^{air}\left(1 - X_{H_2O}^{in}\right), \end{cases} \tag{16}$$

where HR_c is the relative humidity at the cathode inlet and $X_{O_2}^{air}$ is the oxygen molar fraction in the air. Combining (14), (15) and (16), the cathode dynamics write

$$\begin{cases} \frac{dP_{O_2}^c}{dt} = \frac{RT}{V_c}\left(W_c^{in} X_{O_2}^{air}\left(1 - \frac{HR_c P_{sat}(T)}{P_c}\right) - 1 - \frac{HR_c P_{sat}(T)}{P_c}\right) - W_c^{in} X_{O_2}^{air} \frac{S_{cell} N_{cell}}{4F} j \\ \qquad - W_c^{out} \frac{P_{O_2}^c}{P_c}\Big), \\ \frac{dP_{H_2O}^c}{dt} = \frac{RT}{V_c}\Big(W_c^{in} \frac{HR_c P_{sat}(T)}{P_c} - W_c^{out} \frac{P_{H_2O}^c}{P_c} + \frac{S_{cell} N_{cell}}{2F} j \\ \qquad - k_{ad}(\lambda_c)\, c_f \left(\lambda_{eq}^c(P_{H_2O}^c, T) - \lambda_c\right) S_{cell} N_{cell}\Big). \end{cases} \tag{17}$$

2.3.2. Anode gas channels model

The species molar balance at the anode side follows the same rule as at the cathode side. First, we need the molar fraction at the anode inlet. Since an H_2 recirculation is done by an active (pump) or passive (ejector) system, we can assume that we have a complete knowledge of the mixture if we know the recirculation system. The mass conservation of hydrogen and water vapor in the anode gas channels modifies the partial pressures $P^a_{H_2}$ and $P^a_{H_2O}$ in the anode volume through the equations

$$\begin{cases} \dfrac{dP^a_{H_2}}{dt} = \dfrac{RT}{V_a}\left(W^{in}_a X^{in}_{H_2} - \dfrac{S_{cell}N_{cell}}{2F}j - W^{out}_a \dfrac{P^a_{H_2}}{P_a}\right), \\ \dfrac{dP^a_{H_2O}}{dt} = \dfrac{RT}{V_a}\left(W^{in}_a X^{in}_{H_2O} - W^{out}_a \dfrac{P^a_{H_2O}}{P_a} \quad - J^a_w S_{cell}N_{cell}\right). \end{cases} \tag{18}$$

V_a refers to the volume considered for the anode side. W^{in}_a and W^{out}_a refer to the anode inlet and outlet molar flows. $X^{in}_{H_2}$ and $X^{in}_{H_2O}$ are the molar fractions in the anode volume defined by

$$\begin{cases} X^{in}_{H_2O} = HR_a \dfrac{P_{sat}(T)}{P_a}, \\ X^{in}_{H_2} = 1 - X^{in}_{H_2O}, \end{cases} \tag{19}$$

where HR_a is the relative humidity at the anode inlet. Combining (14), (18) and (19), the anode dynamics write

$$\begin{cases} \dfrac{dP^a_{H_2}}{dt} = \dfrac{RT}{V_a}\left(W^{in}_a\left(1 - \dfrac{HR_aP_{sat}(T)}{P_a}\right) - \dfrac{S_{cell}N_{cell}}{2F}j - W^{out}_a\dfrac{P^a_{H_2}}{P_a}\right), \\ \dfrac{dP^a_{H_2O}}{dt} = \dfrac{RT}{V_a}\left(W^{in}_a\dfrac{HR_aP_{sat}(T)}{P_a} - W^{out}_a\dfrac{P^a_{H_2O}}{P_a}\right. \\ \qquad \left. -k_{ad}(\lambda_a)c_f\left(\lambda^a_{eq}\left(P^a_{H_2O},T\right) - \lambda_a\right)S_{cell}N_{cell}\right). \end{cases} \tag{20}$$

Fig. 2 illustrates the full model.

3. Reduced model

We are looking for an accurate and real-time capable observer of the membrane water content. A preliminary study of the PEMFC model described above shows its stability. In other words, even if the membrane water content is initialized with a random value, the model will converge to the same state in large enough time. Nevertheless, the convergence rate is slow, and the main goal of the observer is to speed up the convergence. We observe that the dynamics of the membrane water content is much lower than that of the gas species transport. Therefore, we can consider the cathode and anode pressures as variables whose dynamics is so fast that we can consider the pressure at each time step as a steady state from the mathematical point of view. This results in neglecting the dynamics of the cathode and anode states (17) and (20), namely $\frac{dP^c_{O_2}}{dt} = \frac{dP^c_{H_2O}}{dt} = \frac{dP^a_{H_2}}{dt} = \frac{dP^a_{H_2O}}{dt} = 0$, and expressing it in the semi-explicit form

$$\frac{dx}{dt} = \varphi(x,z,u), \tag{21}$$

$$0 = \psi(x,z,u), \tag{22}$$

with x, z and u the following dynamic and algebraic states and control

$$x = (\lambda_a \ \ \lambda_m \ \lambda_c)^T, \tag{23}$$

$$z = \left(j \ P^c_{O_2} \ P^c_{H_2O} \ P^a_{H_2} \ P^a_{H_2O}\right)^T, \tag{24}$$

$$u = \left(V \ W^{in}_c \ W^{in}_a \ P_c \ P_a HR_c HR_a \ T\right)^T. \tag{25}$$

The three-point water content profile ($\lambda_a \quad \lambda_m \quad \lambda_c$) included in the state variable x denotes a dynamic state while the current j and the partial pressures contained in the state variable z are algebraic states. We specify the PEMFC current as an algebraic state keeping in mind the generalization of the ongoing observer to a future 2D observer model. In fact, most of papers focusing on 2D models emphasize the need for the stack voltage to be an input to the model since it remains constant in the through-channel direction (see Ref. [26]) as compared to the current density which varies. Moreover, considering the current as a state variable does not add much difficulty. The functions φ and ψ respectively include the discretized version of (11) and the stationary version of (17, 20). We then recapitulate the full model, accounting for the strong coupling between the membrane water content variation, the current generation, and the mass balance:

$$\begin{cases} \dfrac{dx}{dt} = \dfrac{D(x)}{\epsilon_1}A_\lambda x + \epsilon_2\begin{pmatrix} -\dfrac{n_d(x)}{F}z_1 + J^a_w(x_1,z_5,u_8) \\ 0\dfrac{n_d(x)}{F}z_1 + J^c_w(x_3,z_3,u_8) \end{pmatrix}, \\ u_1 = E_{rev}(z_2,z_3,z_4,u_8) - \eta_{act}(z_1,z_2,u_8) - \eta_{conc}(z_1,z_2,u_8) - \eta_\Omega(x_2,u_8), \\ \begin{pmatrix} z_2 \\ z_3 \end{pmatrix} = \dfrac{u_2\begin{pmatrix} X^{air}_{O_2}\left(1 - u_6\dfrac{P_{sat}(u_8)}{u_4}\right) \\ u_6\dfrac{P_{sat}(u_8)}{u_4} \end{pmatrix} - \dfrac{z_1}{\epsilon_3}\begin{pmatrix} \frac{1}{2} \\ -1 \end{pmatrix} - \epsilon_4\begin{pmatrix} 0 \\ J^c_w(x_3,z_3,u_8) \end{pmatrix}}{u_2 + \dfrac{z_1}{2\epsilon_3} - \epsilon_4 J^c_w(x_3,z_3,u_8)}, \\ \begin{pmatrix} z_4 \\ z_5 \end{pmatrix} = \dfrac{u_3\begin{pmatrix} 1 - u_7\dfrac{P_{sat}(u_8)}{u_5} \\ u_7\dfrac{P_{sat}(u_8)}{u_5} \end{pmatrix} - \dfrac{z_1}{\epsilon_3}\begin{pmatrix} 1 \\ 0 \end{pmatrix} - \epsilon_4\begin{pmatrix} 0 \\ J^a_w(x_1,z_5,u_8) \end{pmatrix}}{u_3 - \dfrac{z_1}{\epsilon_3} - \epsilon_4 J^a_w(x_1,z_5,u_8)}. \end{cases} \tag{26}$$

with $\epsilon_1 = x_m$, $\epsilon_2 = 1/c_f x_{CL}$, $\epsilon_3 = 2F/S_{cell}N_{cell}$ and $\epsilon_4 = S_{cell}N_{cell}$. With both the cathode and anode pressure dynamics set to zero, the required cathode and anode outlet mass flows needed in (17) and (18) are expressed as

$$W^{out}_c = W^{in}_c + \frac{j}{2F}S_{cell}N_{cell} - J^c_w S_{cell}N_{cell}, \tag{27}$$

$$W^{out}_a = W^{in}_a - \frac{j}{F}S_{cell}N_{cell} - J^a_w S_{cell}N_{cell}. \tag{28}$$

In comparison to Fig. 2, we illustrate the reduced model in Fig. 3. Besides, we define the measured output as

$$y = Cz, \text{ with } C = (1\,0\,0\,0\,0\,0). \tag{29}$$

The output state y is thus be compared to the algebraic variable j to make the observer converge.

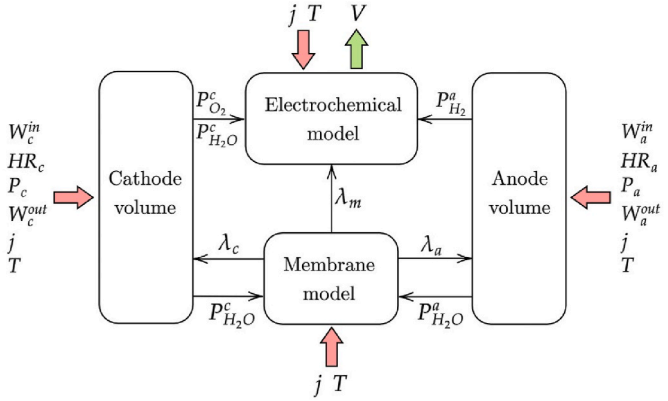

Fig. 2. Recapitulative scheme of the full model.

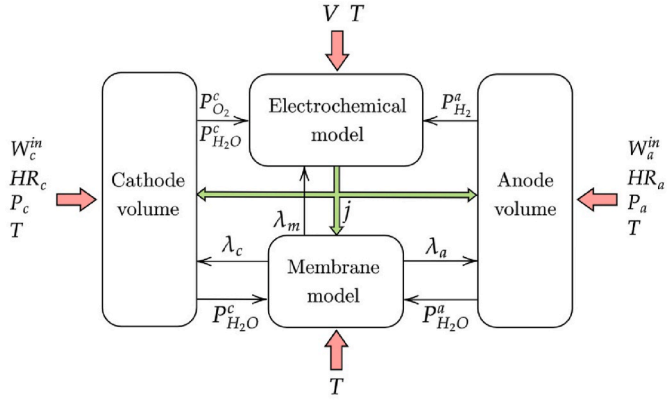

Fig. 3. Recapitulative scheme of the reduced model.

Regarding the operating conditions measurements accessibility included in u, the voltage V and the current j are easy to get, as well as both anode and cathode pressures. Both inlet molar flows and humidities are obtained by modeling of the inlet loops (we do not detail these models as it goes out of the scope of this article). Indeed, sometimes a humidifier is considered from the cathode side while the anode inlet humidity comes from the recirculation loop. We will assume in Section 5 that both inlet molar flow rates W_c^{in}, W_a^{in} are given as well as the inlet cathode humidity HR_c. On the anode side, the anode inlet humidity HR_a is calculated through an ejector modeling.

We numerically verify that we can express the resulting implicit system (21,22) in a common Ordinary Differential Equations (ODE) framework after inverting the algebraic equation (22). This allows us to use classic nonlinear observation strategies. Keeping in mind the usual framework for using nonlinear observers and since we have only discrete measurements, we then rewrite (21,22) as the discrete time system

$$x_{k+1} = f(x_k, u_k), \tag{30}$$

$$y_{k+1} = h(x_{k+1}, u_k). \tag{31}$$

To do this, we first solve system (21,22) numerically through an implicit Euler scheme with a fixed time step, keeping the algebraic equations as a constraint to verify. Given the state x_k and the control u_k, we then perform a Newton method to express at the next iteration the solution (x_{k+1}, z_{k+1}) of the following system

$$x_{k+1} - x_k - \Delta t \varphi(x_{k+1}, z_{k+1}, u_k) = 0, \tag{32}$$

$$\psi(x_{k+1}, z_{k+1}, u_k) = 0. \tag{33}$$

After that, to express the functions f and h involved in the system under the form (30,31), we exhibit $z_{k+1} = \psi_z(x_{k+1}, u_k)$ by solving (33). We straight after numerically invert (32). This leads to express the following functions

$$f(x,u) = (I - \Delta t \varphi(x, \psi_z(x,u), u))^{-1}, \tag{34}$$

$$h(x,u) = C\psi_z(x,u). \tag{35}$$

where I denotes the identity function. Besides, (35) stands for the measurement function involved in (31). The main objective is now to really estimate the dynamic state x according to the ignorance of the initial state x_0. We account for some uncertainties with w_k and v_k, denoting process and observation noises, respectively, which are both assumed to be zero mean multivariate Gaussian noises, with covariance Q_k and R_k, respectively. Having in mind common Kalman filters, the system finally writes in the form

$$x_{k+1} = f(x_k, u_k) + w_k, \tag{36}$$

$$= h(x_{k+1}, u_k) + v_k. \tag{37}$$

4. Adaptive EKF observer

A major drawback of the Extended Kalman Filter (EKF) is the significant impact of the covariance matrices Q_k and R_k on the performance of the filter. In the context of PEMFC estimation, we note that the membrane water content has a dynamic on the order of tens of seconds: large amplitude current variations in a short time interval won't result in large membrane water content variations. Well, the design of covariance matrices R_k and Q_k of the usual EKF does not allow to get a fast observer. Indeed, the common EKF is too sensitive when the current oscillates. In this context, it is relevant to use an adaptive filter such that it has a strong effect when the current is quite stable and a reduced one when the current varies too much. We are inspired by Ref. [22] where the authors design an Adaptive EKF by making adjustment of noise covariance matrices through a coefficient ν. Given the estimated states $(\widehat{x}_{k-1}, \widehat{z}_{k-1})$, the covariance matrices Q_{k-1}, R_{k-1} and the covariance estimate P_{k-1}, we specify the successive steps of the Adaptive EKF as follows:

1. To compute the Jacobian of f involved in (30)

$$F_k = \frac{\partial f}{\partial x}(\widehat{x}_{k-1}, u_{k-1}). \tag{38}$$

2. To get predicted state estimate $\left(\widehat{x}_{k|k-1}, \widehat{z}_{k|k-1}\right)$ solution of (32,33) and compute the Jacobian of h involved in (31)

$$H_k = \frac{\partial h}{\partial x}\left(\widehat{x}_{k|k-1}, u_{k-1}\right). \tag{39}$$

3. To compute the *predicted covariance estimate*

$$P_{k|k-1} = F_k P_{k-1} F_k^T + Q_{k-1}. \tag{40}$$

4. To compute the *measurement residual*

$$d_k = y_k - C\widehat{z}_{k|k-1}, \tag{41}$$

the *residual covariance*

$$S_k = H_k P_{k|k-1} H_k^T + R_{k-1}, \tag{42}$$

and the *resulting Kalman gain*

$$K_k = P_{k|k-1} H_k^T S_k^{-1}. \tag{43}$$

5. To get the *updated state estimate*

$$\widehat{x}_k = \widehat{x}_{k|k-1} + K_k d_k. \tag{44}$$

6. To compute the algebraic solution $\widehat{z}_k$ solution of (33) to be consistent with $\widehat{x}_k$ and the *updated estimate residual*

$$\varepsilon_k = y_k - C\widehat{z}_k. \tag{45}$$

7. To update the *covariance estimate*

$$P_k = (I - K_k H_k) P_{k|k-1}, \tag{46}$$

and get from residuals (41) and (45) the appropriate *covariance matrices*

$$Q_k = \nu Q_{k-1} + (1-\nu)\left(K_k d_k d_k^T K_k^T\right), \tag{47}$$

$$R_k = \nu R_{k-1} + (1-\nu)\left(\varepsilon_k \varepsilon_k^T + H_k P_{k|k-1} H_k^T\right). \tag{48}$$

Note that a larger ν implies that the previous estimates to have more

weight in the computation of Q_k and R_k. Therefore, the observer experiences less fluctuations and longer time delays to catch up with changes. On the contrary a smaller ν implies too much sensitivity to the measures, which can lead to too many oscillations. In our test cases we make a compromise, we choose ν to be 0.5.

5. Results

The membrane water content observer described above becomes useful when load cycles imply noticeable transient variations of the membrane humidity. These oscillatory variations induce an alternating shrinking and swelling behavior that later leads to irreversible physical damages of the membrane [27]. In such cases, the knowledge of the membrane water content allows to close the loop and to adapt the operating conditions in order to stabilize the membrane water content around given safe values, avoiding such oscillatory behavior without the disadvantages of a measuring device. More precisely, we first point out that the designed observer is of great interest during the first seconds, because it quickly converges close to the reference membrane water content, regardless of the initial value of the membrane water content. Then, to illustrate the good performance of the observer, we will present a sensitivity analysis of both the reduced model and the Adaptive EKF. Let us describe the procedure.

5.1. Simulation setup

We use a PEMFC simulation platform in Simcenter Amesim to create the sketch and observe the ability of the designed observer to return the desired variables. The simulation platform consists of several pieces, which are divided into three main parts illustrated in Fig. 4.

- a PEMFC block, whose modeling is described in Section 2;
- a full cathode admission block consisting of a compressor, humidifier and backpressure valve;
- an anode admission block with a primary flow from an H_2 tank and a secondary one from an H_2 recirculation loop through an ejector system. We use a control strategy to give the PEMFC model the correct operating conditions to meet the current demand.

At the stack scale, we choose the several parameters involved in the model description according to the most employed in the literature.

The mass-transfer coefficients for water sorption involved in (14) at the membrane-electrode interfaces is determined by [28].

$$k_{ad}(\lambda) = \begin{cases} a_a f_w \, exp\left[\frac{20000}{R}\left(\frac{1}{T_{ref}} - \frac{1}{T}\right)\right], \lambda < \lambda_{eq} \\ a_d f_w \, exp\left[\frac{20000}{R}\left(\frac{1}{T_{ref}} - \frac{1}{T}\right)\right], \text{else.} \end{cases} \tag{49}$$

The coefficient f_w stands for the water volume fraction in the hydrated ionomer and is given by

$$f_w = \frac{\lambda_m V_w}{\lambda V_w + V_m}, \tag{50}$$

with $V_m = 1/c_f$ being the membrane equivalent volume and V_w the water molar volume. The water diffusivity in the ionomer involved in (11) is given by [28]

$$D(\lambda) = \frac{\mathrm{d}(\lambda_a) + \mathrm{d}(\lambda_c)}{2}, \tag{51}$$

The water electroosmotic drag coefficient is taken as the mean of Springer's original linear law [28] applied to both anode and cathode water content

$$n_d(\lambda) = \frac{\frac{2.5}{22}\lambda_a + \frac{2.5}{22}\lambda_c}{2}. \tag{53}$$

The equilibrium water content involved in the fluxes computing (14) is taken from [29]

$$\lambda_{eq} = \begin{cases} 0.0043 + 17.81 a_{H_2O} - 39.85 {a_{H_2O}}^2 + 36 {a_{H_2O}}^3, \\ 14 + 1.4(a_{H_2O} - 1), 1 < a_{H_2O} < 3 \\ 16.8, a_{H_2O} > 3 \end{cases} \tag{54}$$

The coefficient σ_p involved in (9) is taken from [24] which used a N117 Nafion membrane

$$\sigma_p(\lambda_m) = (0.005139\lambda_m - 0.00326)\exp\left[\frac{E_{memb}}{R}\left(\frac{1}{T_{ref}} - \frac{1}{T}\right)\right]. \tag{55}$$

The bulk oxygen diffusion coefficient involved in (7) is computed following [30] with the formula

$$D_{O_2} = \frac{1}{D_{O_2-N_2} + D_{O_2,\mathrm{Kn}}}, \tag{56}$$

with $D_{O_2-N_2}$ the binary diffusion coefficient of O_2 and N_2 and $D_{O_2,\mathrm{Kn}}$ the Knudsen O_2 coefficient. No flooding is considered in this diffusive transport model. Then, the effective diffusion coefficient remains constant throughout the GDL. We recapitulate the used parameters in Table 1 which are inspired from one of our test cases.

The parameters in Table 1 are typical of either the fuel cell geometry or the electrochemistry. Given experimental data, these different

Table 1
Values of several constants involved in the modeling.

$P_{ref} = 1.013$ bar	$T_{ref} = 298.15$ K
$E_{act} = 66000$ Jmol^{-1}	$E_{memb} = 10542$ Jmol^{-1}
$S_{cell} = 320$ cm^2	$N_{cell} = 320$
$c_f = 1818$ molm^{-3}	$x_m = 25$ µm
$x_{CL} = 15$ µm	$x_{GDL} = 15$ µm
$j_0^{ref} = 1.015 \times 10^{-3}$Acm^{-2}	$\alpha = 0.5635$
$a_a = 3.53 \times 10^{-3}$cms^{-1}	$a_d = 3.53 \times 10^{-3}$cms^{-1}
$P_{O_2}^{ref} = 0.21$bar	

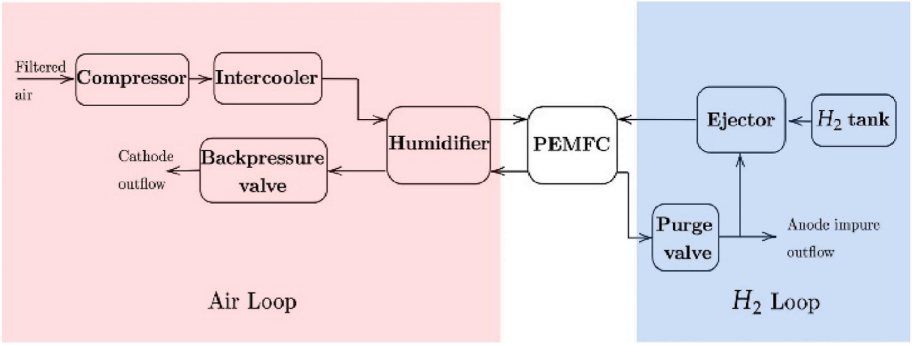

Fig. 4. Block scheme of a PEMFC system for a functioning vehicle whose simulation platform is designed with Simcenter Amesim software.

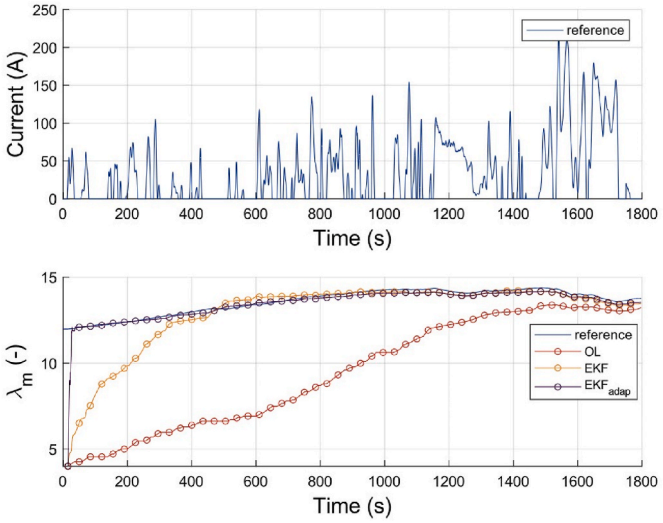

Fig. 5. Membrane water content on a WLTC use-case: reference (blue), open loop (red) and respectively EKF closed loops with or without adaptive gain (orange and purple). (For interpretation of the references to color in this figure legend, the reader is referred to the Web version of this article.)

parameters can be used as fitting parameters to make the model fit the data. The choice of parameters to be used depends on the user's knowledge of the fuel cell under consideration.

5.2. Simulation results

We highlight the observer's ability on a "Worldwide Harmonized Light Vehicles Test Cycles" (WLTC) example with an initial membrane water content of 12 (see Fig. 5), which gives a reference trajectory. Along this trajectory, the membrane water content increases up to a given value and stays around that value. In real life, we have no way of knowing the initial membrane water content. Therefore, the error made at the starting point with such a random value converges to zero very slowly (as the system is stable). We claim that the observer designed upon reduces this error much faster.

We illustrate this in Fig. 5, which shows both the shortcomings of the open-loop model and the advantages of the closed-loop model, when we have no information about the initial water content of the membrane. Starting from a random value, the open-loop value of the membrane water content converges to the reference value. However, the convergence remains slow, and we need more than 20 min to be in an acceptable range of values. Therefore, the lack of precision of the open-loop model may result in a poor estimate of the membrane water content for a significant interval. In comparison, the closed-loop membrane water content needs only a few seconds to approach the reference membrane water content, regardless of the initial membrane water content.

To highlight the effectiveness of the Adaptive EKF approach, we implement a standard EKF observer for comparison. The results show that the Adaptive EKF convergence is faster.

In Fig. 5, we note that the membrane water content is very stable. We explain this phenomenon through the air loop calibration that we construct to account for a stable cathode relative humidity at the inlet. To highlight the observer's ability to recover the membrane water content when it varies, in Fig. 6 we perform a comprehension test where the current demand is fixed at 100A and the cathode relative humidity at the inlet varies. We observe the same performance as in Fig. 5. The observer converges faster than the open loop when we start from an unknown initial water content. In addition, the observer can track humidity changes.

In Fig. 7, we plot the first moments of the Adaptive EKF applied to the WLTC use case, starting from different initial values. Regardless of the starting point, we observe that the filter quickly approaches the reference membrane water content compared to the open-loop model. We also notice a small gap between the reference and observed values depending on the initial value chosen, which is negligible when looking at the gap with the open-loop value. At lower initial values, e.g., 4, the observer is a bit slower. We explain this by the fact that the observer is completely ineffective when the current is zero. We can't get any information when there is no current. Well, we note that at the beginning of the WLTC case, the current is not important and is often zero. Finally, the observer of the membrane water content becomes relevant when we do not have measuring device of the humidity and no idea of the water content at the starting time t.

In conclusion, only with current and voltage measurements, cathode and anode pressures and mass flow rates, the designed observer allows to recover the membrane water content in a few seconds, regardless of the initial value.

Finally, let us mention that the Adaptive EKF designed is about ten times faster than real time with a Python implementation of the model on a personal computer (2.6 GHz CPU).

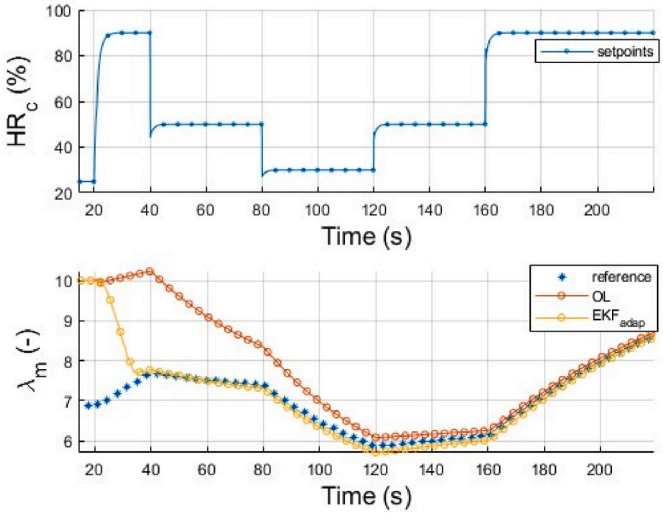

Fig. 6. Membrane water content on a comprehension's test (current $I = 100A$, $HR_c \in (30, 90)$): reference (blue), open loop (red) and AEKF (orange). (For interpretation of the references to color in this figure legend, the reader is referred to the Web version of this article.)

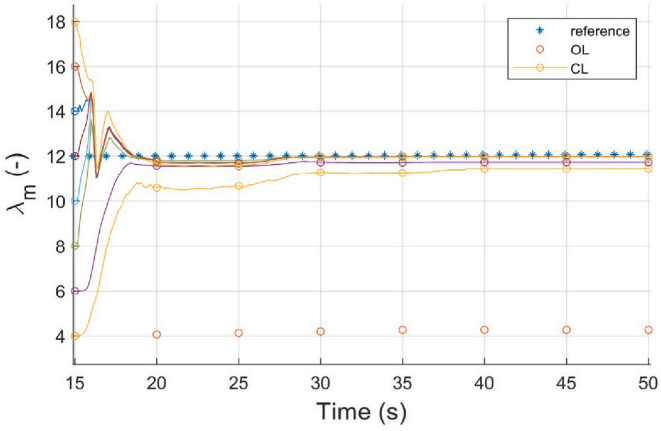

Fig. 7. Membrane water content: reference value (stars) and open loop values (circles) and Adaptive EKF starting from several values (circles with lines).

Table 2
Sensitivity analysis: inputs standard deviations.

Input variables	3 σ-value	unit
Voltage (V)	1	V
Current (I)	1	A
Pressures (P_a,P_c)	30	mbar
Cathodic inflow (W_c^{in})	5%	Kgs^{-1}
Anodic inflow (W_a^{in})	5%	Kgs^{-1}
Temperature (T)	1	K
Inlet humidities (HR_a,HR_c)	5%	(−)

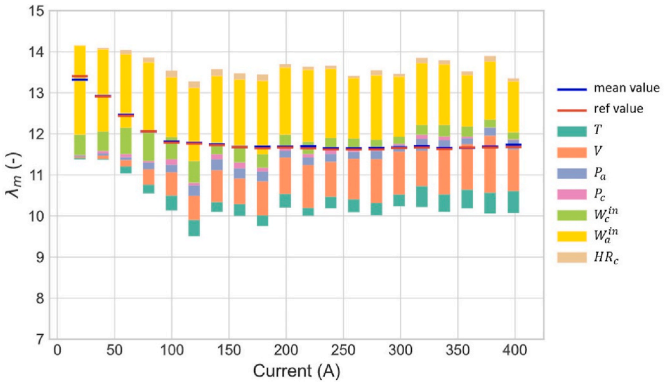

Fig. 8. Reduced model sensitivity analysis to input data.

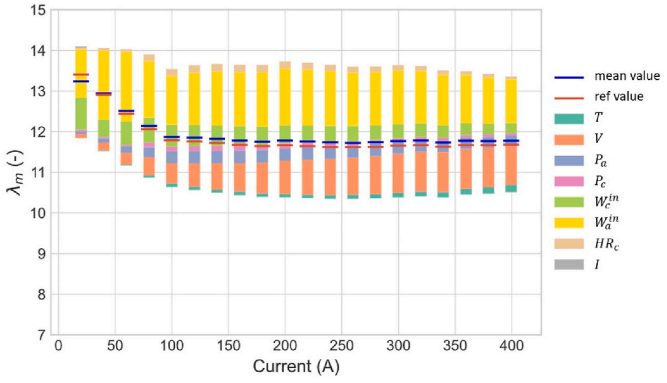

Fig. 9. Adaptive EKF sensitivity analysis to input data.

5.3. Sensitivity analyses

Our goal is to use the designed observer for real-time observation in operating cycles. To ensure the observed states to be in suitable range of values, we perform a sensitivity analysis of the reduced model with respect to the input data included in the control variables u, whose scatter values are stored in Table 2. The 3 σ scatter values are representative of the usual industrial sensor's accuracy.

We then plot in Fig. 8 the resulting scattered membrane water content with respect to several current values from 0 to 400A. The min-max values of the bars represent the global scatter of the estimated membrane water content. The contribution of each scattered input data is represented by different colors. The larger is the colored area, the greater the impact of the corresponding input scatter on the output accuracy. This figure highlights that the model is sensitive to the input accuracies. Nevertheless, the obtained dispersion of the membrane water content is still acceptable (3σ around $\pm$ 1.5). We notice that regardless of the current values, the scatter of the membrane water content is primarily falling to the anode inflow's accuracy. We find that overall accuracy is not sensitive to the range of current values, although it is slightly less scattered for small current values.

In addition, we verify in Fig. 9 that the closed-loop system is not more sensitive to uncertainties than the open-loop model by plotting a sensitivity analysis of the closed-loop system. In addition to the already mentioned scattered inputs, the current is also an input of the observer. We confirm that the scattered current does not affect the closed loop.

We explain this by the choice of the Kalman filter which is supposed not to be sensitive to measurement noise. Compared to Fig. 8, the standard deviation of the membrane content is not much lower. We also notice that temperature has a weaker effect than in the open-loop modeling. Finally, we notice that the mean membrane water content in Fig. 9 slightly differs from the reference value. We explain this by the following fact: for a given value of membrane water content, the current of the reduced model is slightly different from that of the full model, which corresponds to the current measured as the input of the closed loop. The Adaptive EKF makes the output current to be close to the measured one, which means that the membrane water content as the output of the closed loop is slightly different from the reference value. In summary, both sensitivity analyses are similar, and the closed-loop modeling confirms that the observer does not add uncertainties to the modeling.

5.4. Discussion and perspectives

Firstly, we observe that the designed observer allows for the estimation of the membrane water content in the fuel cell using reachable outputs such as the current and voltage without the need for dedicated sensors. In addition, we notice that the Adaptive EKF converges to the original value faster than the open-loop or the common EKF, regardless of the initial membrane water content chosen. This feature is particularly useful when adjusting control laws, especially during the initial start-up phase when users lack information about the humidity levels inside the fuel cell. It is important to note that the closed loop value may not be the same as the reference value, but it remains within an acceptable range. It is necessary to determine the intake molar flows, which can be achieved with either real sensors or independent software sensors. To demonstrate the model's sensitivity to input and measures, we conduct a sensitivity analysis on both stationary points and transient cycles for both the reduced model and the Adaptive EKF. These analyses confirm the reliability of the observer in relation to the confidence we have in the input variables. Based on the scattered entries gathered in Table 2, we conclude that the standard deviation of the observed membrane water content is approximately 0.5 regardless of the current value.

To make things even better, we are aware that there is a growing interest in 2D modeling of the PEMFC in real time (see Refs. [26,31]). To this end, the PEMFC modeling constructed in this article lays the foundations for further multidimensional observation strategies. Indeed, as illustrated in Fig. 3, we choose to make current an output of the system rather than an input. This choice is motivated by the fact that pseudo-2D modeling requires the voltage to be an input, since it remains constant throughout the discretization in the through-the-channel direction. We expect that the computation time will be the primary challenge in extending the real observer to pseudo-2D modeling.

Regrading other observational issues, it is worth mentioning that the water content of the membrane is sensitive to the temperature. In the sensitivity analysis, we only consider a standard deviation of one degree. However, it should be noted that a temperature gradient of approximately five degrees can be observed inside a fuel cell between the exhaust and the membrane core. Therefore, it is worth noting to consider temperature modeling in conjunction with humidity modeling in the cell.

Finally, the chosen modeling only deals with single-phase water management. Liquid water is of interest for both efficiency and potential damage. Improving the model by considering liquid water as an additional state to be estimated would be beneficial.

6. Conclusions

In this paper, we develop a software sensor to monitor the water content in the membrane of a PEMFC. This model-based observer considers the main transport phenomena occurring in the membrane. Thus, it provides more accurate information about the behavior of the moisture in the membrane of the fuel cell during operation.

Compared with physical sensors, which may not be suitable for all PEMFC systems, we develop a software sensor that can be easily adapted to the PEMFC and the selected auxiliaries.

Finally, the software sensor is less sensitive to input data than the model it is based on. The designed observer has a standard deviation of 0.5, which means a coefficient of variation of 5%. This precise observer can operate in real-time, allowing other users to construct control laws to adapt fuel cell humidity.

7. Funding agencies

This research did not receive any specific grant from external funding agencies in the public, commercial, or not-for-profit sectors.

CRediT authorship contribution statement

Gontran Lance: Writing – review & editing, Writing – original draft, Methodology, Investigation. **Thomas Leroy:** Writing – review & editing, Writing – original draft, Investigation, Conceptualization. **Jules Sery:** Writing – original draft, Investigation.

Declaration of competing interest

The authors declare that they have no known competing financial interests or personal relationships that could have appeared to influence the work reported in this paper.

References

[1] IEA. Net zero by 2050. Paris: IEA; 2021.
[2] Barbir F, Görgün H, Wang X. Relationship between pressure drop and cell resistance as a diagnostic tool for PEM fuel cells. J Power Sources 2005;141(1):96–101. https://doi.org/10.1016/j.jpowsour.2004.08.055.
[3] Li H, Tang Y, Wang Z, Shi Z, Wu S, Song D, et al. A review of water flooding issues in the proton exchange membrane fuel cell. J Power Sources 2008;178(1):103–17. https://doi.org/10.1016/j.jpowsour.2007.12.068.
[4] Hong P. Water content estimation and control of PEM fuel cell stack and the individual cell in vehicle. Singapore: Springer Nature Singapore; 2022.
[5] Tang Z, Huang Q-A, Wang Y-J, Zhang F, Li W, Li A, et al. Recent progress in the use of electrochemical impedance spectroscopy for the measurement, monitoring, diagnosis and optimization of proton exchange membrane fuel cell performance. J Power Sources 2020;468:228361. https://doi.org/10.1016/j.jpowsour.2020.228361.
[6] Debenjak A, Gašperina M, Petrovčič. On-line tracking of fuel cell system impedance using extended kalman filter. In: Zio E, editor. PHM 2013 special issue. Milano: AIDIC; 2013. p. 1003–8.
[7] Diab Y, Auger F, Schaeffer E, Chevalier S, Allahham A. Real-time estimation of PEMFC parameters using a continuous-discrete extended kalman filter derived from a pseudo two-dimensional model. Energies 2022;15(7):2337. https://doi.org/10.3390/en15072337.
[8] Wei Y, Zhao Y, Yun H. Estimating PEMFC ohmic internal impedance based on indirect measurements. Energy Sci Eng 2021;9(8):1134–47. https://doi.org/10.1002/ese3.878.
[9] Chinnavat T, Chanin P. Estimation of water content in PEM fuel cell. Chiang Mai J Sci 2008;35(1):212–20.
[10] Görgün H, Arcak M, Barbir F. An algorithm for estimation of membrane water content in PEM fuel cells. J Power Sources 2006;157(1):389–94. https://doi.org/10.1016/j.jpowsour.2005.07.053.
[11] Böhler L, Ritzberger D, Hametner C, Jakubek S. Constrained extended Kalman filter design and application for on-line state estimation of high-order polymer electrolyte membrane fuel cell systems. Int J Hydrogen Energy 2021;46(35):18604–14. https://doi.org/10.1016/j.ijhydene.2021.03.014.
[12] Zhang X, Pisu P. An unscented kalman filter based on-line diagnostic approach for PEM fuel cell flooding. Int J Prognostics Health Manag 2014;5(1). https://doi.org/10.36001/ijphm.2014.v5i1.2204.
[13] Luna J, Husar A, Serra M. Nonlinear distributed parameter observer design for fuel cell systems. Int J Hydrogen Energy 2015;40(34):11322–32. https://doi.org/10.1016/j.ijhydene.2015.05.132.
[14] Cecilia A, Serra M, Costa-Castelló R. Nonlinear adaptive observation of the liquid water saturation in polymer electrolyte membrane fuel cells. J Power Sources 2021;492:229641. https://doi.org/10.1016/j.jpowsour.2021.229641.
[15] Cecilia A, Astolfi D, Costa-Castelló R. A new nonlinear observer for liquid water estimation in fuel cells. IEEE Trans. Contr. Syst. Technol. 2023:1–12. https://doi.org/10.1109/TCST.2023.3337512.
[16] Piffard M, Gerard M, Da Fonseca R, Massioni P, Bideaux E. Sliding mode observer for proton exchange membrane fuel cell: automotive application. J Power Sources 2018;388:71–7. https://doi.org/10.1016/j.jpowsour.2018.03.057.
[17] Kazmi IH, Bhatti AI. Parameter estimation of Proton Exchange Membrane Fuel Cell system using sliding mode observer. International Journal of Innovative Computing Information and Control 2012;Volume 8(Number 7(B)):5137–48.
[18] Jiao J, Chen F. Adaptive sliding mode kalman observer for the estimation of vehicle fuel cell humidity. In: SAE technical paper series. SAE International400 commonwealth drive; 2022. Warrendale, PA, United States.
[19] Long R, Chen Q, Zhang L, Ma L, Quan S. Online soft sensor of humidity in PEM fuel cell based on dynamic partial least squares. TheScientificWorldJOURNAL 2013;2013:923901. https://doi.org/10.1155/2013/923901.
[20] Jiao J, Chen F. Humidity estimation of vehicle proton exchange membrane fuel cell under variable operating temperature based on adaptive sliding mode observation. Appl Energy 2022;313:118779. https://doi.org/10.1016/j.apenergy.2022.118779.
[21] Chi X, Chen F, Jiao J. Model-based observer for vehicle proton exchange membrane fuel cell humidity based on adaptive sliding mode estimation technique. Int J Hydrogen Energy 2024;52:750–66. https://doi.org/10.1016/j.ijhydene.2023.04.165.
[22] Akhlaghi S, Zhou N, Huang Z. Adaptive adjustment of noise covariance in Kalman filter for dynamic state estimation. IEEE Power & Energy Society General Meeting. IEEE; 2017. p. 1–5. 2017 - 2017.
[23] Kulikovsky AA. Analytical modeling of fuel cells. Elsevier; 2019.
[24] Springer TE, Zawodzinski TA, Gottesfeld S. Polymer electrolyte fuel cell model. International Journal of Energy and Environmental Engineering 1991;138(8). https://doi.org/10.1149/1.2085971.
[25] Vetter R, Schumacher JO. Experimental parameter uncertainty in proton exchange membrane fuel cell modeling. Part I: scatter in material parameterization. J Power Sources 2019;438:227018. https://doi.org/10.1016/j.jpowsour.2019.227018.
[26] Goshtasbi A, Pence BL, Chen J, DeBolt MA, Wang C, Waldecker JR, et al. A mathematical model toward real-time monitoring of automotive PEM fuel cells. J Electrochem Soc 2020;167(2):24518. https://doi.org/10.1149/1945-7111/ab6dd1.
[27] Ren P, Pei P, Li Y, Wu Z, Chen D, Huang S. Degradation mechanisms of proton exchange membrane fuel cell under typical automotive operating conditions. Prog Energy Combust Sci 2020;80:100859. https://doi.org/10.1016/j.pecs.2020.100859.
[28] Vetter R, Schumacher JO. Free open reference implementation of a two-phase PEM fuel cell model. Comput Phys Commun 2019;234:223–34. https://doi.org/10.1016/j.
[29] O'Hayre R, Cha S-W, Colella W, Prinz FB. Fuel cell fundamentals. Hoboken, NJ, USA: John Wiley & Sons, Inc; 2016.
[30] Das PK, Jiao K, Wang Y, Barbir F, Li X. Fuel cells for transportation: fundamental principles and applications. Woodhead Publishing; 2023.
[31] Goshtasbi A, Pence BL, Ersal T. Computationally efficient pseudo-2D non-isothermal modeling of polymer electrolyte membrane fuel cells with two-phase phenomena. J Electrochem Soc 2016;163(13):F1412–32. https://doi.org/10.1149/2.0871613jes.